Research

Maturation of pyramidal cells in anterior piriform cortex may be sufficient to explain the end of early olfactory learning in rats

Enver Miguel Oruro,[1,2,3,6] Grace V.E. Pardo,[2,4,5,6] Aldo B. Lucion,[4] Maria Elisa Calcagnotto,[2,3] and Marco A. P. Idiart[1,3]

[1]Neurocomputational and Language Processing Laboratory, Institute of Physics, Universidade Federal do Rio Grande do Sul, Porto Alegre, RS, 91501-970 Brazil; [2]Neurophysiology and Neurochemistry of Neuronal Excitability and Synaptic Plasticity Laboratory, Department of Biochemistry, Institute of Basic Health Sciences, Universidade Federal do Rio Grande do Sul, Porto Alegre, RS, 90035-003 Brazil; [3]Neuroscience Graduate Program, Universidade Federal do Rio Grande do Sul, Porto Alegre, RS, 90050-170 Brazil; [4]Department of Physiology, Institute of Basic Health Sciences, Universidade Federal do Rio Grande do Sul, Porto Alegre, RS, 90050-170 Brazil; [5]Centre for Interdisciplinary Science and Society Studies, Universidad de Ciencias y Humanidades, Los Olivos, Lima, 15314 Peru

Studies have shown that neonate rodents exhibit high ability to learn a preference for novel odors associated with thermo-tactile stimuli that mimics maternal care. Artificial odors paired with vigorous strokes in rat pups younger than 10 postnatal days (P), but not older, rapidly induce an orientation-approximation behavior toward the conditioned odor in a two-choice preference test. The olfactory bulb (OB) and the anterior olfactory cortex (aPC), both modulated by norepinephrine (NE), have been identified as part of a neural circuit supporting this transitory olfactory learning. One possible explanation at the neuronal level for why the odor-stroke pairing induces consistent orientation-approximation behavior in <P10 pups, but not in >P10, is the coincident activation of prior existent neurons in the aPC mediating this behavior. Specifically, odor-stroke conditioning in <P10 pups may activate more mother/nest odor's responsive aPC neurons than in >P10 pups, promoting orientation-approximation behavior in the former but not in the latter. In order to test this hypothesis, we performed in vitro patch-clamp recordings of the aPC pyramidal neurons from rat pups from two age groups (P5–P8 and P14–P17) and built computational models for the OB-aPC neural circuit based on this physiological data. We conditioned the P5–P8 OB-aPC artificial circuit to an odor associated with NE activation (representing the process of maternal odor learning during mother–infant interactions inside the nest) and then evaluated the response of the OB-aPC circuit to the presentation of the conditioned odor. The results show that the number of responsive aPC neurons to the presentation of the conditioned odor in the P14–P17 OB-aPC circuit was lower than in the P5–P8 circuit, suggesting that at P14–P17, the reduced number of responsive neurons to the conditioned (maternal) odor might not be coincident with the responsive neurons for a second conditioned odor.

At an early stage of postnatal development, infant rats show a high ability to learn artificial odors associated with tactile stimuli that mimic maternal care. Younger pups (P5–P8) conditioned by pairing a novel scent with vigorous strokes on their backs (using a soft brush) show a consistent orientation-approximation behavior toward the conditioned odor (Moriceau and Sullivan 2005; Morrison et al. 2013; Roth et al. 2013; Ghosh et al. 2015). Interestingly, in older pups (P14–P17) the odor-stroke conditioning protocol did not induce the same behavior (Moriceau and Sullivan 2005; Morrison et al. 2013; Roth et al. 2013; Ghosh et al. 2015). Why does the odor-stroke pairing lose its ability to induce preference to the conditioned odor? Possible answers to this question were offered based on the underlying neural mechanisms of the behavioral phenomena.

It has been proposed that the relevant neural circuit includes the OB and the aPC, both modulated by the NE released from the locus coeruleus (LC). The pairing of odor with activation of β-adrenoceptors in the OB (Sullivan et al. 1992) or in the aPC (Morrison et al. 2013; Ghosh et al. 2015, 2017) induces behavioral olfactory preference in younger infant rodents (rat and mice), while the blocking of these receptors or the lesioning of the LC before pairing (Sullivan et al. 1994) prevents it.

In the LC-OB circuit, it has been suggested that developmental changes in the LC might be in part responsible for the failure of the odor-stroke conditioning in inducing olfactory preference learning in older infant rats. For neonates, LC presents a large response to somatosensory stimuli (noxious and nonnoxious) (Kimura and Nakamura 1985), which no longer occurs in >P10 pups (Rangel and Leon 1995). This functional maturational change in the LC–NE system appears to be dependent on the emergence of the LC autoinhibitory function due to the increase of the NE inhibitory autoreceptor α2 and to the decrease of the autoexcitatory function mediated by NE α1 autoreceptors. Indeed, the pharmacological blockage of the α2 autoreceptors and the activation of the

α1 autoreceptors in older pups, during odor presentation, reinstates the odor preference learning (Moriceau and Sullivan 2004).

Another possible explanation focuses on the OB-aPC circuit, specifically at the level of sensory synapses. Sensory information from OB is projected to the aPC by the lateral olfactory tract (LOT), formed by the axons of the mitral and tufted cells. LOT terminals end at the superficial layer of aPC (L1a), forming sensory synapses on the apical dendrites of the pyramidal cells with somas positioned at deep layers (L2 and L3). The L2 and L3 layers and the second portion of the superficial layer (L1b) receive inputs from associative regions, including autoassociative projections (Bekkers and Suzuki 2013). At an early stage of development, high synaptic plasticity at the LOT–L1a aPC synapses is observed, which declines around the first month of postnatal life (Poo and Isaacson 2007) possibly due to down-regulation of NMDA receptors (Franks and Isaacson 2005). Furthermore, it has been found that LOT–L1a plasticity is modulated by β-adrenoceptors induced an increase of L-type calcium channel (LTCC) currents, and that may not be true for older pups (Ghosh et al. 2017).

One hypothesis is that younger rat pups (<P10) learn the mother's odor by associative processes inside the nest (Moriceau and Sullivan 2005). The neural circuit that supports the conditioned learning of artificial odors in experimental conditions (Moriceau and Sullivan 2005) must be the same involved in natural learning in the nest. According to this view, the initially neutral maternal odor (CS) activates a specific group of pyramidal neurons in the aPC, while the maternal care (UCS) elicits a larger response in the pyramidal neurons via the LC–NE system. The repeated natural "pairing" of maternal odor with maternal care (through providing warmth, feeding, touching, licking) causes these neurons to become responsive to the conditioned maternal odor alone and promotes the behavioral approximation. Thus, the response of the neural circuit to the mother's odor in the 1-wk-old pup is completely different from the response to the same stimuli in the newborn rat. Based on this assumption, we offer here an alternative answer for the behavioral olfactory learning phenomena in infant rat pups based on the intrinsic developmental characteristics of the aPC pyramidal cells of younger (<P10) and older pups (>P10).

We hypothesize that odor-stroke conditioning in P5–P8 pups recruits a group of aPC pyramidal cells that are also activated by the maternal odor. As this neural circuit promotes approximation to the maternal odor, we assume their coincidental activation also promotes behavioral preference for the conditioned odor. However, this occurs only for younger pups (<P10). For >P10 pups, the odor-stroke conditioning results in less activation of

the aPC pyramidal cells and, therefore, limited chances of recruitment of cells that are also responsive to maternal odor.

To test this hypothesis, we perform a patch-clamp electrophysiological experiment to characterize the intrinsic passive and active properties of the aPC pyramidal cells in two periods of postnatal development (P5–P8 and P14–P18). Then, using the parameters obtained from the experimental data, we implement a computational model of the OB-aPC circuit for the two age periods with a pyramidal cell model that represents the intrinsic properties of real pyramidal cells. Finally, we simulate the process of maternal odor learning inside the nest in the computational OB-aPC model and test the responsiveness of the circuits to the conditioned maternal odor. After conditioning, we expect a lower activation to the presentation of the conditioned maternal odor for P14–P17 aPC pyramidal cells than for P5–P8 aPC.

Results

Patch-clamp electrophysiological data of L2/3 aPC pyramidal cells

Whole-cell patch-clamp recordings were performed from 21 L2/3 pyramidal cells from P5–P8 and P14–P17 age rat pups. As for other sensorial cortices in development, both the passive and active electrophysiological properties of aPC L2/3 pyramidal cell were significantly changed with age (Table 1). In addition, we examined the spike frequency evoked by depolarizing current pulses 500 msec long. The minimum current required for spike train induction (Rheobase) increased significantly with development. At P5–P8, a +40 pA step current-induced spikes in all cells tested ($n = 9$), but at P14–P17, +90 pA or more was needed ($n = 12$). The input–output relationship was examined by plotting the spike frequency versus the amplitude of the injected current (Fig. 1). Pyramidal cells from P5–P8 increased rapidly their spiking frequency reaching their maximum spiking frequency at lower current steps (+60 pA–+120 pA), and after that, the spiking frequency of the cells remained relatively steady despite the increase in the intensities of current injection. On the other hand, cells from P14–P17 reach their maximum spiking frequency at higher current steps (+180pA–+200 pA), and this continued to increase proportionally to the injected current.

Computational model of aPC pyramidal cells

The computational models of P5–P8 and P14–P17 aPC pyramidal cells were calibrated by optimizing their parameters to reproduce

Table 1. Passive and active electrophysiological properties of L2/3 aPC pyramidal neurons

Parameters	P5–P8 ($n = 9$ cells)		P14–P17 ($n = 12$ cells)		$t_{(19)}$	P
	Mean ± SEM	SD	Mean ± SEM	SD		
Passive membrane properties						
V_{rest} (mV)	−39.22 ± 1.89	5.66	−54.35 ± 0.66	2.27	8.45	<0.0001****
R_{in} (MΩ)	438.6 ± 33.15	99.44	177.1 ± 14.44	50.02	7.91	<0.0001****
$τ_m$ (ms)	42.78 ± 4.17	12.53	30.33 ± 1.69	5.88	3.04	0.007**
C_m (pF)	98.21 ± 7.16	21.48	178.1 ± 10.83	37.51	5.70	<0.0001****
Active membrane properties						
AP threshold, (mV)	−36.63 ± 1.35	4.04	−45.96 ± 1.80	6.24	3.90	0.001**
AP amplitude (mV)	76.90 ± 3.38	10.13	85.43 ± 4.53	15.69	1.42	0.17
AP half-amplitude width (ms)	4.32 ± 0.33	0.98	2.97 ± 0.09	0.34	4.46	0.0003***
Max. frequency (Hz)	11 ± 2.36	7.07	21.50 ± 2.53	8.79	2.94	0.0085**
Rheobase (pA)	48.89 ± 6.76	20.28	95.00 ± 11.04	38.26	3.27	0.004**
AP threshold -V_{rest} (mV)	3.92 ± 2.95	8.86	8.77 ± 2.38	8.23	1.29	0.21

Intrinsic properties were measures through whole-cell current clamp of L2/3 aPC pyramidal cells at P5–P8 and P14–P17. Values are mean ± SEM or SD. Asterisks represent statistically significant unpaired Student's t-test comparisons. **$P < 0.01$; ***$P < 0.001$; ****$P < 0.0001$.
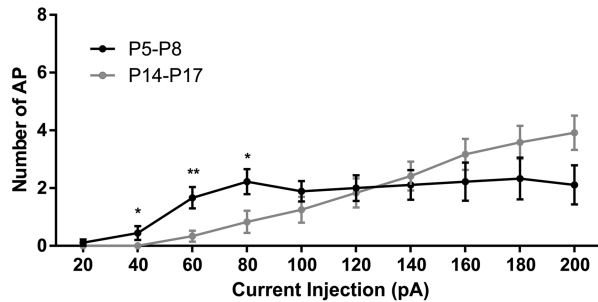
Figure 1. Number of AP-current injected curves of aPC L2/3 pyramidal cells in P5–P8 and P14–P17age rat pups. A relationship between the average number of AP and intensity of injected current (pA) in a 200 msec window recording in brain slices from P5–P8 (black curve, $n = 9$ cells) and P14–P17 (gray curve, $n = 12$ cells) aged pup rats. Asterisks represent statistically significant unpaired Student's t-test comparisons between P5–P8 and P14–P17 at each current intensity. (*) $P < 0.05$; (**) $P < 0.01$.

the characteristics of the two age groups. In Figure 2 the adjusted, postoptimized, model of aPC pyramidal cells is shown superimposed (blue) to the experimental data (colors) of the spike numbers as a function of current injection for P5-P8 (A, $n = 9$ records from nine cells) and P14–P17 (B, $n = 12$ records from 12 cells) and for the ISI-current injection relationship obtained from adjusted experimental data (black) for P5–P8 (C, $n = 7$ records from seven cells) and P14–P17 (D, $n = 11$ records from 11 cells). The average injected current that evoked only two spikes was considered for the first ISI adjusted point. For P5–P8 it was 70 pA, and for P14–P17 it was 126 pA, with average ISI values of 56.6 and 107.23 msec, respectively. For the second and third ISI adjusted points, we considered arbi-

trary representative current injections of 140 and 200 pA, and the ISI average values were obtained from the first two spikes evoked by those currents. For P5–P8, the ISI adjusted point for 140 pA was 31.95 msec, and at 200 pA was 22.17 msec. For P14–P17, the ISI adjusted point at 70 and 140 pA were 62.6 and 37.1 msec, respectively.

We next tested if the distinct pyramidal cells properties of P5–P8 and P14–P17 are still conserved when the adjusted models are included in the OB-aPC circuits. In the OB-aPC circuits, one pyramidal cell receives random excitatory inputs from 20 to 140 mitral cells, and we simulate synaptic change at the Mt–Pyr synapses for 6000 msec. In Figure 3, the change of input dependent weight in pyramidal cells in OB-aPC circuits is shown superimposed for the two age groups in 13 circuits (colors). In P5–P8, the circuit of 20 Mt–Pyr induced an important reduction in the synaptic weight (42.85% from the basal value) (A1, red curve below the dotted line) and circuits with 30–140 Mt–Pyr gain synaptic weight (34%–54% from the basal value) (A1, colors curve above the dotted line). In P14–P17, circuits of 20, 30, and 40 Mt–Pyr induced an important reduction in the synaptic weight (42.85% from the basal value) (A2, color curves below the dotted line), while circuits of 50–180 Mt–Pyr induced a great gain (37%–57% from the basal value).

A plot of individual circuits comparing the weight change in the two ages is shown in Figure 3B. The aPC pyramidal cells receiving inputs from 20 Mt cells present a decrease in synaptic weight, independently of age interval (B1); as the number of Mt inputs increase, we observe a sharp transition after which there is an important increase in synaptic change. For pyramidal cells in the P5–P8 age interval, the transition occurs at approximately 30 Mt inputs, while for P14–P17 at approximately 50 Mt inputs (B1–B9).

A comparative plot of the average of synaptic weight as a function of Mt inputs is shown in Figure 3C. Circuits of 50 Mt–Pyr gain
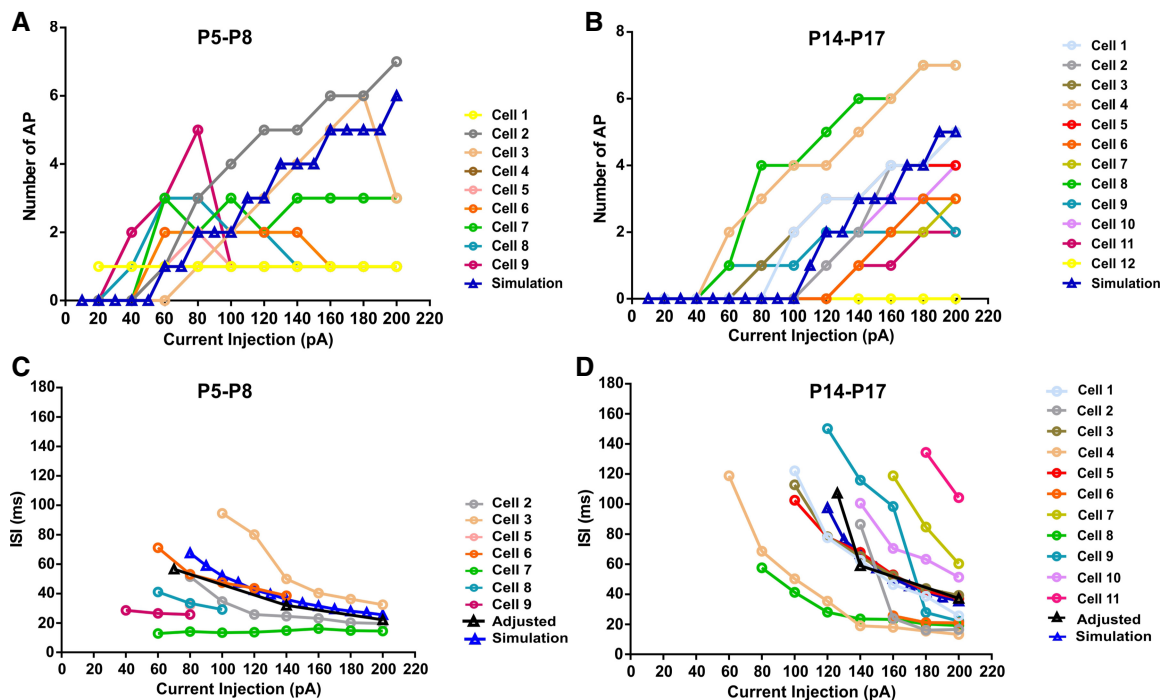

Figure 2. Representative results of current-clamp analysis and simulation of experimental data. Current injection versus the number of AP from individual pyramidal cells in current-clamp recording at (*A*) P5–P8 and at (*B*) P14–P17. Colors represent different pyramidal cells measured in intervals of 20 pA. Note the variability in cell response for different current injections. The blue curve represents the simulated data based on the adjusted curve. (*C*) Current injection versus interspike interval (ISI) from individual pyramidal cells at P5–P8 and (*D*) P14–P17 in a 200 msec window recording. Each point and color represents the value of each individual pyramidal cell obtained in current-clamp recording from cells with two or more spikes in a given current injection. The black curve (triangle) represents three adjusted points chosen to represent the experimental ISI mean curve for each age group (*C,D*).
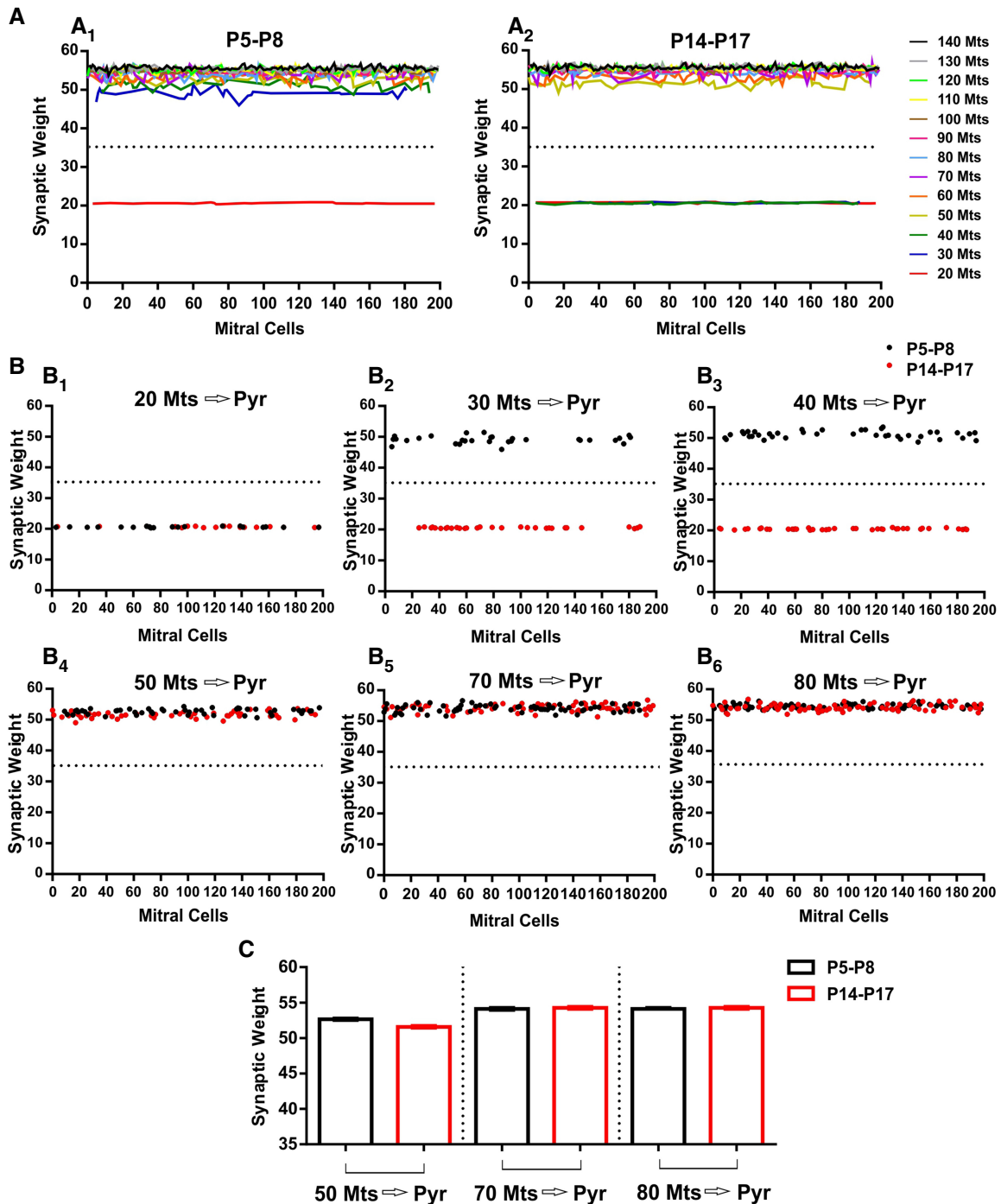
Figure 3. Simulation of plasticity weight change at mitral-pyramidal cells synapses across 6000 msec simulation period for P5–P8 and P14–P17 age group. The circuit formed by 200 mitral cells and 13 pyramidal cells was simulated during 15 respiratory cycles. Each pyramidal cell receives random inputs from 20 to 80 mitral cells firing at respiratory rhythm of 2 Hz (color curves), and their activities induce changes in the synaptic weights of the OB-aPC circuit (*A*). Inputs from 30 to 140 mitral cells (*A1*) or from 50 to 140 mitral cells (*A2*) induce gain in synaptic weight (plotted from synaptic weight before simulation, 35) at P5–P8 and P14–P17, respectively. Note that only inputs from 20 mitral cells induce loss of synaptic weight in pyramidal cells from the P5–P8 group, but inputs from 30 or more induce a great gain of synaptic weight (*B1*), which occurs with 50 or more mitral cells inputs for the P14–P17 age group (*B1–B6*). When we look closer at the circuit when the two-age groups gain synaptic weight (*C*), we can note that 50 Mt–Pyr circuits gain more weight in the P5–P8 group than in the P14–P17 group and as the number of mitral cells inputs increase (70 and 80 Mt–Pyr circuits), the gain of synaptic weight become similar for the two ages.

more synaptic weight in P5–P8 (52.66 ± 0.12, $n = 50$) than in P14–P17 (51.58 ± 0.14, $n = 50$) [$t_{(98)} = 5.83$, $P < 0.0001$, unpaired Student's *t*-test]. On the other hand, circuits of 70 Mt–Pyr

(P5–P8: 54.12 ± 0.14, $n = 70$ vs. P14–P17: 54.27 ± 0.14, $n = 70$) or 80 Mt–Pyr (P5–P8: 54.18 ± 0.12, $n = 80$ vs. P14–P17: 54.50 ± 0.07, $n = 80$) show a similar gain of synaptic weight ($P > 0.05$, unpaired

Student's *t*-test). These results indicate that in both circuits P5–P8 and P14–P17, the pyramidal cells still conserved their properties to respond to depolarizing inputs and correspondingly gain synaptic plasticity. However, in the continuum development of circuits, what will happen with synaptic modifications induced by Mt depolarizing inputs when the aPC pyramidal cells properties change with the maturation from P5–P8 to P14–P17?

We next tested whether the gain in synaptic plasticity observed in P5–P8 circuits is still conserved when parameters of the pyramidal cells switch from the P5–P8 to the P14–P17. In Figure 4A, we see the change in the resting membrane potential of three

pyramidal cells receiving input from 50 random mitral cells (Cell 1, Cell 2, and Cell 3, superimposed orange, green, and blue traces) when their intrinsic electrophysiological properties switch from P5–P8 to P14–P17. After the switch, the Cell 1 reduces in 50% its firing frequency, and after 1700 msec of simulation, it stops (B1). Cell 2 (B2) and Cell 3 (B3) also reduce their firing frequency after the switch but remain active until the end of the simulation.

In Figure 4C, we see the average of synaptic weight change for circuits with 30 Mt–Pyr, 40 Mt–Pyr, and 70 Mt–Pyr cells. Pyramidal cells receiving inputs from 30 Mt cells experienced an increase in synaptic strength with P5–P8 parameters (49.07 ± 0.21, $n = 30$,
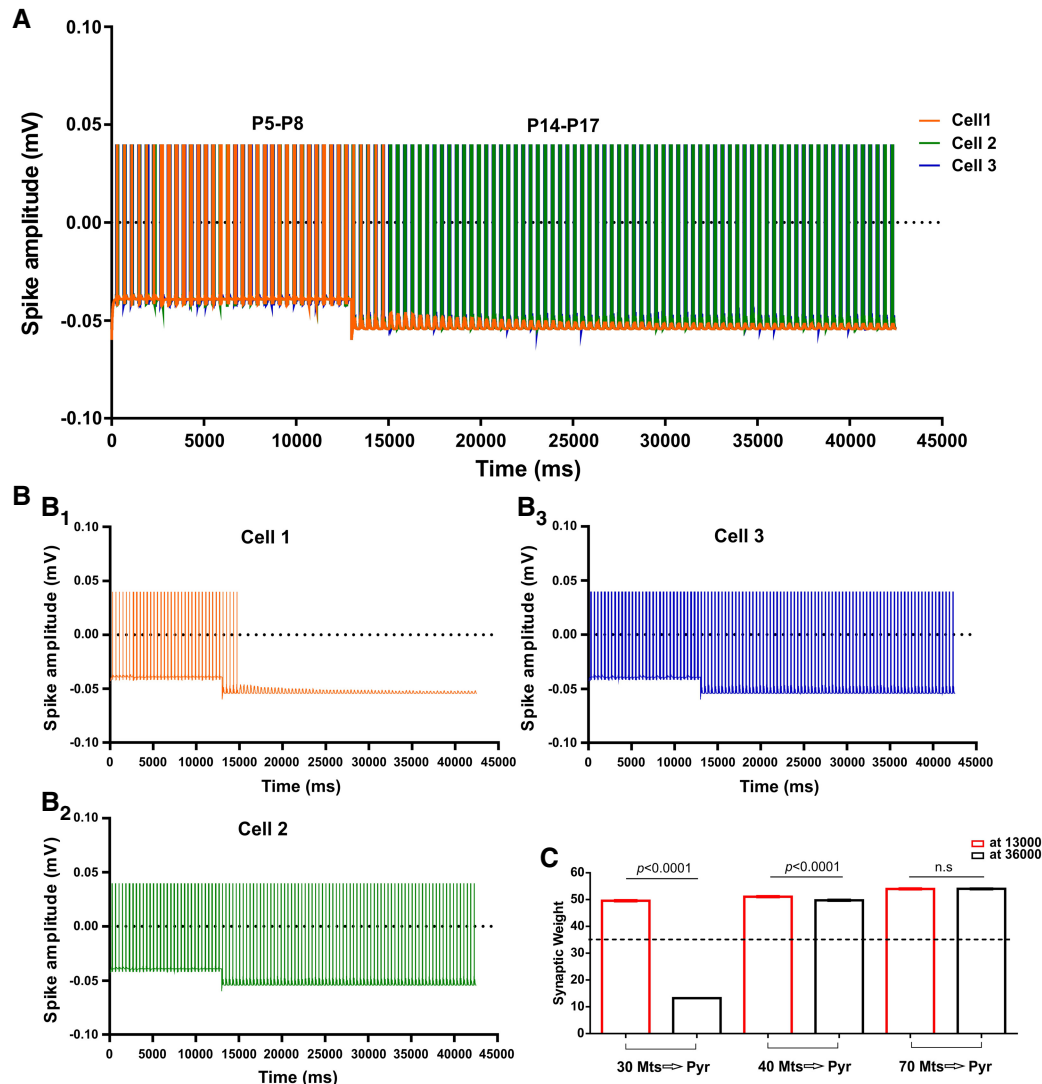

Figure 4. Simulation of the evoked activity in aPC pyramidal cells during the switch in intrinsic properties from P5–P8 to P14–P17. We simulate the Mitral-Pyramidal circuit and the evoked spikes of three random choices of pyramidal cells (color traces) recorded when receiving input from 50 random mitral cells firing at respiratory rhythm of 2 Hz (*A*). Initially, the passive and active membrane properties of these pyramidal cells were set up to represent the profile of the P5–P8 age period and after approximately 10,000 msec of simulation, the passive and active properties membrane properties of pyramidal cells were switched to represent the profile of P14–P17 age period. Note the large hyperpolarization in the resting membrane potential of the three neurons during the change of their membrane potential values, which continues steadily until the end of the simulation. Interestingly, the Cell 1 (orange traces) stops its firing after the switch of membrane properties values, but the Cell 2 (green trace), and Cell 3 (blue trace) continue to firing steadily until the end of the simulation. In the same simulation, we recorded the synaptic changes of those pyramidal cells receiving inputs from 30, 40, and 70 random mitral cells (*C*) and recorded the average of synaptic weight at the end of 13,000 msec (red bar) and 36,000 msec (black bar) of simulation. Pyramidal cells receiving inputs from 30 mitral cells show a synaptic weight gain after 13,000 msec but not after 36,000 msec. On the other hand, the pyramidal cell receiving inputs from 40 and 70 mitral cells show a steady synaptic gain during all simulation periods. Δt: 0.5 msec; Bin: 0.5 msec.
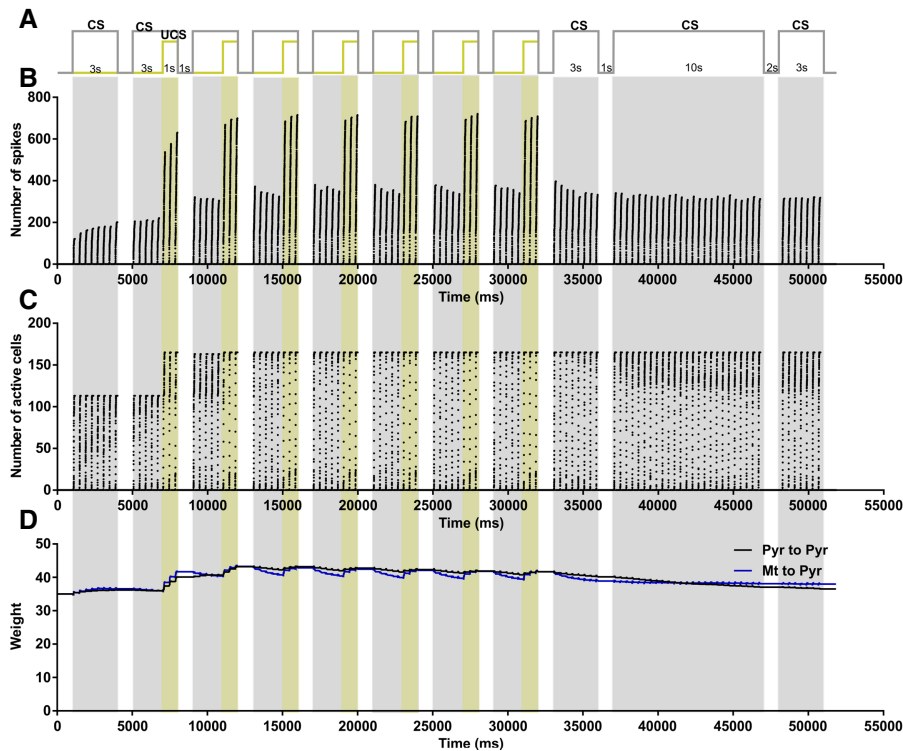
Figure 5. Simulation of the maternal odor preference's learning and exposure to the conditioned maternal odor in P5–P8 aPC pyramidal cells. (*A*) Protocol for classical conditioning of maternal odor preference in the nest. A delayed pairing procedure was used in which the CS (maternal odor) onset preceded the UCS (maternal care, NE action) by 2 sec. CS and UCS overlapped for 1 sec, after which the CS was terminated. The CS–UCS pairing was presented seven times with 1 sec intervals. Learning was tested by the presentation of CS during 3 sec. After the test, CS alone was presented again during 10 sec. After a 2-sec interval learning was tested again by the presentation of CS during 3 sec. During this period, the pyramidal cells of the aPC had properties compatible with the P5–P8 age. (*B*) Number of cumulative aPC pyramidal cell spikes during the CS–UCS pairing and CS presentation, collected at every 100 msec of simulation. (*C*) Number of active aPC pyramidal cells during the CS–UCS pairing and CS presentation, collected at every 100 msec of simulation. (*D*) Synaptic weight gain of Pyr–Pyr (black curve) and Mt–Pyr (blue curve) synapses during CS–UCS pairing and CS presentation. Excitatory mitral inputs fire at the respiratory rhythm (2 Hz). Bin 0.5 msec.

conditioned OB-aPC model to the conditioned odor (CS) in two conditions: (1) The model has parameters compatible with P5–P8 age (Fig. 5), and (2) the model parameters switch from the P5–P8 to the P14–P17 profile (Fig. 6). In Figure 5, the change in pyramidal cells activity and weight at the Mt–Pyr synapses during conditioning and odor exposure protocol (A) are shown in cumulative dots registered at every 200 msec of simulation. After the conditioning, the number of spikes and the number of active Pyr cells in response to CS increases (B and C) compared to the CS before the conditioning. These changes were maintained steady during the CS presentation (10 msec) (B and C).

Moreover, after conditioning, the synaptic strengths increased at Mt–Pyr (blue curve), Pyr–Pyr synapses (black curve), and this gain was maintained during CS presentation (D). This result indicates that P5–P8 OB-aPC circuits modify their synaptic plasticity, number of active cells, and spikes in response to the conditioned odor because of training. However, in nature, the rodent pups learn the mother's odor during the first postnatal days (<P10), and this learned odor is tested in >P10 age pups. What will happen at the circuit level with synaptic modifications induced by maternal odor learning when the aPC pyramidal cell properties change with the maturation from P5–P8 to P14–P17?

Next, we repeated the classical conditioning protocol, but this time, after the test of the CS odor, we switched the intrinsic properties of the aPC pyramidal cells to the P14–P17 age profile before submitting the circuit to the CS odor exposure protocol (Fig. 6A). After conditioning, the behavior of the network is similar to Figure 5. But this time, the prolonged exposure to the CS odor results in a gradual reduction in the number of pyramidal spikes (Fig. 6B), the number of active cells (Fig. 6C), and synaptic strength at Mt–Pyr but not at Pyr–Pyr synapses (Fig. 6D).

Figure 7 shows the comparative changes in the number of pyramidal spikes (A) and the number of active pyramidal cells (B) after the conditioning CS test and during CS odor presentation in the switched P14–P17 circuit (red dots) superimposed on the nonswitched P5–P8 circuit (black dots). During CS odor presentation, the pyramidal cells from the switched circuit (P14–P17) showed an important reduction in the number of spikes compared to pyramidal cells from the nonswitched circuit (P5–P8) (A). Similarly, during CS odor presentation, the number of active pyramidal cells was dramatically reduced in the switched circuit (P14–P17) compared to the nonswitched (P5–P8) (B). These results indicate that when the properties of cells mature from P5–P8 to P14–P17, the P5–P8 circuits that have learned the maternal odor lose plasticity at the level of the OB-aPC synapses, as well as the number of active pyramidal cells and spikes in response to the maternal odor. Together these results suggest that the P14–P17 OB-aPC circuits may have a reduced number of pyramidal cells responsive to the maternal odor.

measured at 13,000 msec of simulation, black bar) but suffered a decrease when the parameters changed to the P14–P17 profile (20.57 ± 0.03, measured at 36,000 msec, red bar) [$t_{(58)} = 131.8$, $P < 0.0001$, unpaired Student's *t*-test]. On the other hand, pyramidal cells receiving inputs from 40 Mt cells show an increase in synaptic weight with P5–P8 parameters (51.08 ± 0.17, $n = 40$, measured at 13,000 msec of simulation, black bar). After the switch to the P14–P17 profile the average of synaptic weight (49.75 ± 0.17, $n = 40$, measured at 13,000 msec of simulation, red bar) was above the basal value and slightly smaller than for the P5–P8 profile [$t_{(78)} = 5.55$, $P < 0.0001$, unpaired Student's *t*-test]. On the other hand, pyramidal cells receiving inputs from 70 Mt cells exhibited a gain in synaptic strength independent of the age profile [P5–P8: 54.00 ± 0.16, $n = 70$ vs. P14–P17: 54.01 ± 0.13, $n = 70$; $t_{(138)} = 0.04$, $P = 0.97$, unpaired Student's *t*-test]. These results indicate that circuits that have gained synaptic connections at P5–P8 induced by a given Mt input lost it after the properties of pyramidal cells switched to the P14–P17 profile in response to the same input.

Responses to the presentation of the conditioned odor

First, we submitted the P5–P8 OB-aPC model to a classical conditioning protocol (odor-stroke) to simulate the process of learning the pup preference for the mother's odor. Then we exposed the
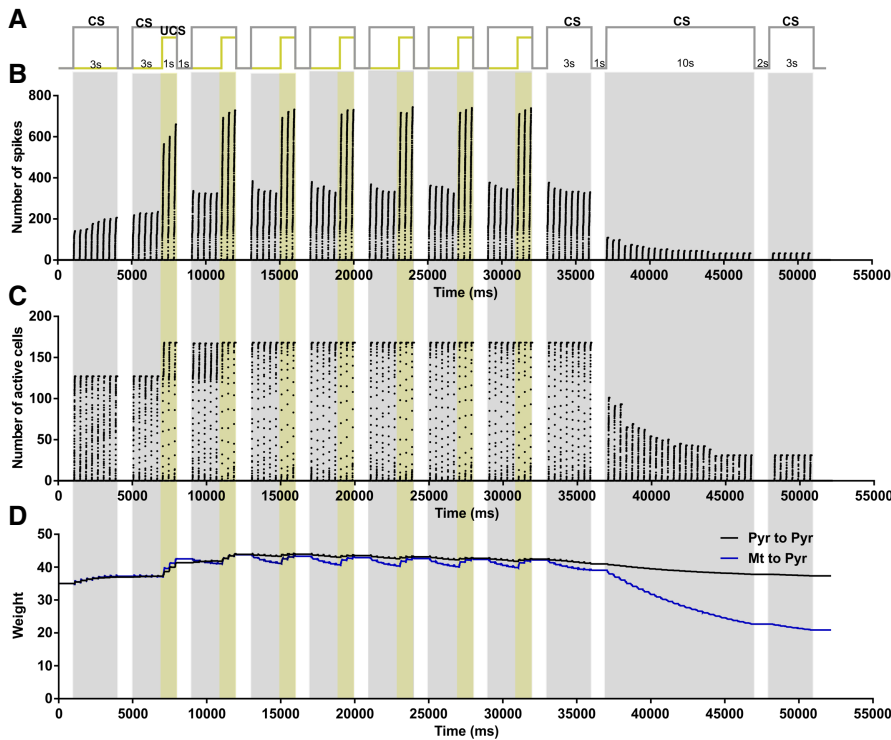
Figure 6. Simulation of maternal odor preference learning in P5–P8 aPC pyramidal cells and exposure to the conditioned maternal odor in P14–P17 aPC pyramidal cells. (*A*) Protocol for classical conditioning of maternal odor preference in the nest. A delayed pairing procedure was used in which the CS (maternal odor) onset preceded the UCS (maternal care, NE action) onset by 2 sec. CS and UCS overlapped for 1 sec, after which the CS was terminated. The CS–UCS pairing was presented seven times with 1s intervals for the network with aPC having parameters compatible with the P5–P8 age. Learning was tested by the presentation of CS during 3 sec. After the test, the network had its parameters shifted to the P14–P17 age and the CS alone was presented again during 10 sec. After 2-sec of interval, learning was tested again by the presentation of CS during 3 sec. (*B*) Number of cumulative aPC pyramidal cell spikes during the CS–UCS pairing and CS presentation, collected at every 100 msec of simulation. (*C*) Number of active aPC pyramidal cells during the CS–UCS pairing and CS presentation, collected at every 100 msec of simulation. (*D*) Synaptic weight gain of Pyr–Pyr (black curve) and Mt–Pyr (blue curve) synapses during CS–UCS pairing and CS presentation. Excitatory mitral inputs fire at the respiratory rhythm (2 Hz). Bin 0.5 msec.

Discussion

Intrinsic membrane properties of aPC pyramidal cells change from P5–P8 to P14–P17, and the number of cells reduces gradually in response to the exposure to the conditioned maternal odor

Younger infant rats (<P10) rapidly learn olfactory preference to a novel odor paired with a vigorous stroke on their back, but the pairing of the same stimuli did not induce this learning in older pups (>P10) (Moriceau and Sullivan 2005). Here we explore whether the odor-stroke conditioning is effective in inducing olfactory preference learning in younger pups because it activates more aPC pyramidal cells responsive to the maternal odor that promotes an orientation-approximation behavior that no longer occurs in older pups. Given that intrinsic membrane properties of pyramidal cells determine the integration of the synaptic inputs and ultimately the action potential generation, we hypothesized that in older pups (P14–P17), there are fewer aPC pyramidal cells responsive to maternal odor than in younger pups (P5–P8) due to their intrinsic maturational properties.

To address this question, we examined the membrane and AP properties of aPC pyramidal cells of rat pups of P5–P8 and P14–P17. We found in aPC slices that L2/3 pyramidal cells in older pups had

reduced resting membrane potential, input resistance, and membrane time constant compared to younger pups. Moreover, action potentials (AP) in older pups had a higher hyperpolarizing threshold and more rapid APs than in younger pups. In older pups, higher step amplitudes of depolarizing current were needed to elicit action potentials, and the frequency of their firing increased as the step of current injection amplitude increased. The aPC pyramidal cells of younger pups evoked APs at lower amplitude steps of depolarizing current injection, and after reaching the maximum frequencies of firing, these cells showed a rapid adaptation in their firing frequency. Using characteristics of real cells, we constructed an artificial model of the P5–P8 and P14–P17 OB-aPC circuits and simulated the learning of the maternal odor inside the nest using a classical conditioning paradigm, and after that, we simulated the exposure of the circuits to the conditioned maternal odor. We found that aPC cells from the P5–P8 circuit showed a greater number of active aPC pyramidal cells and spiking responses during the exposure (10 sec) to the maternal odor, while the aPCs from P14–P17 showed a gradual reduction in the number of active aPC pyramidal cells and spiking responses during the exposure to the same stimuli.

Processing of the OB synaptic inputs in the aPC pyramidal cells at P5–P8 and P14–P17

One of the main findings in this study is that the number of aPC pyramidal neurons responsive to the conditioned maternal odor (the neurons that mediate orientation-approximation behavior) decreases with age due to maturational changes in the intrinsic properties of the aPC pyramidal cells. Our proposed explanation is that in older pups (P14–P17) the reduced number of aPC pyramidal neurons responsive to the maternal odor, might be not overlapping with the aPC pyramidal neurons responsive to a second conditioned odor and that this might be more likely to occur when they are younger (P5–P8). We also propose that the different results for odor-stroke conditioning in infant rats at <P10 and >P10 can be explained by the developmental changes in the intrinsic membrane properties of the target aPC pyramidal cells, which have a lower threshold for synaptic inputs from the OB in P5–P8 than in P14–P17. It has been suggested that pyramidal cells with a higher input resistance and prolonged time membrane constant have responses of greater magnitude and prolonged duration for the synaptic input (McCormick and Prince 1987). Therefore, aPC pyramidal cells from younger rats with these intrinsic electric characteristics, would respond better to synaptic inputs with small currents and slow kinetics, while these cells in older pups have more hyperpolarized resting membrane potential, reduced input resistance and faster membrane time constant responding better to prolonged synaptic inputs with higher currents with faster kinetics. Therefore, a novel odor-stroke conditioning in older pups did not induce olfactory preference learning.
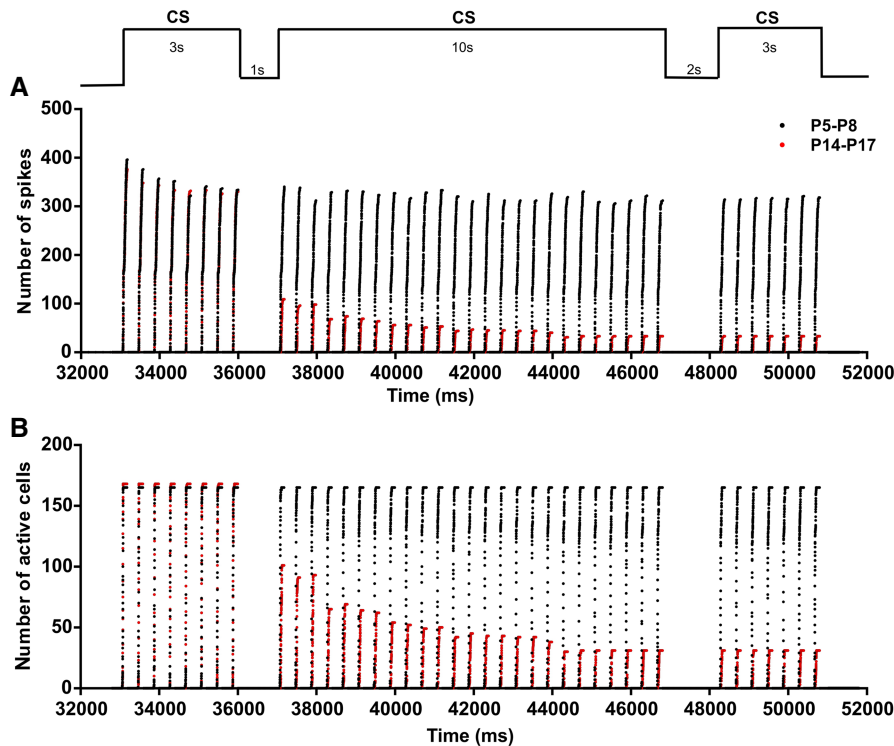
Figure 7. Comparison of the number of spikes and number active cells in P5–P8 and P14–P17 aPC pyramidal cells evoked by conditioned maternal odor. After the conditioning of CS (maternal odor) and UCS (maternal care) in an artificial olfactory circuit with aPC pyramidal cells with passive and active electrophysiological characteristics of P5–P8 rats, the evoked response of pyramidal cells to CS alone was tested in the same age circuit (first CS in *A,B*). In order to compare the evoked pyramidal cells to conditioned maternal odor at P5–P8 and P14–P17, the CS alone was presented again (second CS in *A,B*) 1 sec after the first CS was finished and 2 sec after the second CS was finished (third CS in *A,B*). (*A*) The number of spikes with characteristics of P5–P8 was higher in response to CS alone (black points). On the other hand, the evoked response of pyramidal cells characteristic of P14–P17 was reduced progressively throughout the CS presentation (red points). The same evoked response was observed for the two age group cells during the third CS presentation. (*B*) The reduced spike activity at P14–P17 in response to CS was due to the reduction in the number of active pyramidal cells compared with P5–P8. Excitatory mitral inputs fire at the respiratory rhythm (2 Hz). Bin 0.5 msec.

Maternal odor preference learning is supported by the same circuit that supports early olfactory preference learning for an artificial odor

Our simulation of learning represents the current understanding that rodent pups learn maternal odor through experiences with the mother inside the nest during the first postnatal week. Neonate rats (P1–P4) tested in two-choice tests show organized orientation-approximation behavior toward the maternal odor in relation to nest bedding (Polan and Hofer 1998; Polan et al. 2002), nest bedding in relation to clean bedding (Cornwell-Jones and Sobrian 1977; Szerzenie and Hsiao 1977) and the maternal diet odor in relation to standard diet (Duveau and Godinot 1988). Older pups (in the second and third postnatal weeks) continued to show consistent preferences to the maternal odor (Polan and Hofer 1998; Al Aïn et al. 2016; Perry et al. 2016), to their own nest bedding (Gregory and Pfaff 1971; Cornwell-Jones and Sobrian 1977), and to the maternal diet odor (Duveau and Godinot 1988; Terry and Johanson 1996). All this behavioral evidence suggests that associations formed inside the nest between the maternal/nest odor and a range of maternal care stimuli (warmth, feeding, touching, licking) mediate the olfactory preference learning for the mother/nest's odor (Moriceau and Sullivan 2005). Therefore, at birth, the mother's odor may be a neutral stimulus that elicits little more than an orienting response in pups, and only after a period inside the nest, does the mother's odor becomes effective in eliciting an orientation-approximation behavior in the pup.

It has been proposed that maternal odor learning is the same that supports the conditioned learning of artificial odor outside the nest (paired with stroke and tactile stimuli that mimic maternal licking stimulation) (Sullivan 2001). Thus, in the newborn rat, the neutral maternal odor may elicit the activity of specific groups of pyramidal neurons in the aPC, while maternal care may elicit a great response in the pyramidal neurons via the LC–NA system. The repeated natural "pairing" of maternal odor with maternal care during mother–infant interactions elicits the activity of groups of aPC pyramidal neurons. After a few days, these neurons become responsive only to the conditioned maternal odor and promote behavioral approximation. Therefore, the response of the neural circuit to the mother's odor in the 1 wk pup would be completely different from the response to the same stimuli in the newborn rat.

Future Work

In this work, we show a change in the activity of the aPC pyramidal cells in the OB-aPC circuit for two age periods as a function of the connections of mitral cells with pyramidal cells, where the activity of the mitral cells for both age circuits was the same. To control the number of variables in the experimental model, we made some simplifying assumptions. First of all, some cells types were not included, like the axonal terminal from the olfactory nerve (olfactory sensory neurons), periglomerular cells and granule cells in the OB circuit, the feedforward and feedback interneurons in the aPC circuit (cf. de Almeida 2013, 2016). Additionally, developmental distinctions in the inhibitory synaptic inputs to the aPC pyramidal cells in the two age groups (Pardo et al. 2018) were also not included.

Similarly, we have omitted the NE modulation of the LOT-aPC synapses proposed to mediate the enhanced synaptic excitation and reduced inhibition underlying early odor preference learning in <P10 (Ghosh et al. 2015). The excitatory synaptic plasticity has not been modeled in Mitral-Pyramidal synapses, another developmental difference between these periods (higher at an early postnatal period and progressively declining around the first month (Poo and Isaacson 2007)) as a function of the downregulation of NMDA receptors at LOT-aPC synapses (Franks and Isaacson 2005). Some of these variables could be relevant to prevent the early odor preference learning in P14–P17 infant rats and are left for future work.

We constructed OB-aPC circuits for P5–P8 and P14–P17 rats, in which we modeled similar spontaneous activity of Mt cells for the two periods. Moreover, during the simulation of conditioning and odor presentation protocols, the Mt cells were modeled to fire at a constant frequency for the two circuits and each pyramidal cell

to receive inputs from 15–45 random Mt cells. Higher inputs from Mt cells to aPC pyramidal cells (>80) may enable P14–P17 infant rats to learn the preference for the novel odor paired with stroke. However, as semilunar cells (SL), whose somas are more superficially located in layer 2 of the piriform cortex (Bekkers and Suzuki 2013), do not have autoassociative connections (Choy et al. 2017), they could be more affected by the reduction in number of aPC pyramidal cells responsive to conditioned maternal odor than the deeper pyramidal cells with autoassociative properties studied here.

Our model does not exclude the other reasons for the odor-stroke conditioning lack of effectiveness in inducing olfactory preference in older pups (i.e., development of the LC–NE system, development of LOT-aPC synaptic plasticity). Instead, our hypothesis adds to these previous findings in explaining the phenomenon. During the maturation of the olfactory system many scenarios may occur. The one we adopt here is due to the maturation of the aPC pyramidal cells, as observed in our experiments, and it is a straightforward and comprehensive hypothesis.

Contributions of the model to the odor-stroke conditioning outcomes in infant rats

The results presented here can help us to understand at a neural level the behavioral outcomes of odor-stroke conditioning in <P10 and >P10 rat pups. In the classical conditioning paradigm adopted for younger rat pups (P5–P8), the unconditioned stimulus is a vigorous stroke on the pup's back, which after repeated pairing with an odor (the conditioned stimulus) induces the behavioral response of approximation toward the conditioned odor. Interestingly, the stroke did not elicit this response before training, only an increase in the motor basal activity of the pups (Sullivan et al. 1986; Sullivan and Wilson 1993). However, how can a novel odor become effective in eliciting an approximation response when it has been paired with a tactile stimulus that did not elicit this response? Our answer for that is to consider that the odor-stroke pairing takes advantage of the circuitry in aPC already developed during the pup`s interactions with the mother in the nest. In other words, the properties of the immature pyramidal cells in aPC allow the odor-stroke conditioning to recruit a circuit that partially overlaps with the circuit supporting the approximation behavior toward the mother`s odor. With the maturation of the pyramidal cells in the aPC after P10 the overlap in the circuits is no longer possible, and the odor-stroke pairing is no longer effective. We think that this is the most straightforward hypothesis given the knowledge of the circuitry, and it is an experimentally testable hypothesis. This approach would also be supported by the unified reinforcement principle proposed by Donahoe et al. (2006), in which the respondent/operant behavior emerges simultaneously inside the nest. From this perspective, the neurons recruited for the conditioned maternal odor in the aPC could be the same activated during the odor-stroke conditioning, and these coincident neurons would be the ones that are reduced in the P14–P17 OB-aPC circuit in the simulation of the maternal odor exposure.

In conclusion, our model suggests two distinct functions for odor processing in the OB-aPC circuit for the associative learning in <P10 and >P10 infant rats based on the development of intrinsic electrophysiological properties of aPC pyramidal cells. For the two developmental OB-aPC circuits, the success for the odor-stroke pairing is dependent on the coincidental activation during conditioning of the aPC pyramidal cells responsive to the maternal odor promoting orientation-approximation behavior (Fig. 8). The change in the intrinsic properties of the aPC pyramidal cells reduces the availability of the maternal odor responsive pyramidal cells during the maternal odor exposure.

Materials and Methods

Experimental procedures

Animals and ethics statement

Electrophysiological data were obtained from Wistar rat pups in two age groups (P5–P8 and P14–P17) from the Centre for Reproduction and Animal Experimentation Laboratory of the Universidade Federal do Rio Grande do Sul (UFRGS). Animals were housed under controlled temperature ($21 \pm 1°C$) and humidity (60%) conditions and were maintained on a 12-h light–dark schedule (lights on at 06:00 h) with free access to water and rodent chow (Nuvilab Cr2). Animal use and all experimental procedures were in concordance with the Guidelines for Animal Care and Use of Laboratory Animals of the National Institute of Health and were approved by the Ethics Committee in Use of Animals (CEUA) of UFRGS (Number 27961/2014).

Patch–clamp current–clamp recording

For electrophysiological studies, slices of aPC were prepared from male and female Wistar rat pups at age P5–P8 and P14–P17 as described previously (Pardo et al. 2018). Whole-cell patch-clamp recordings were made on pyramidal cells located in the L2/3 of aPC under the mode of current-clamp with axon Multiclamp
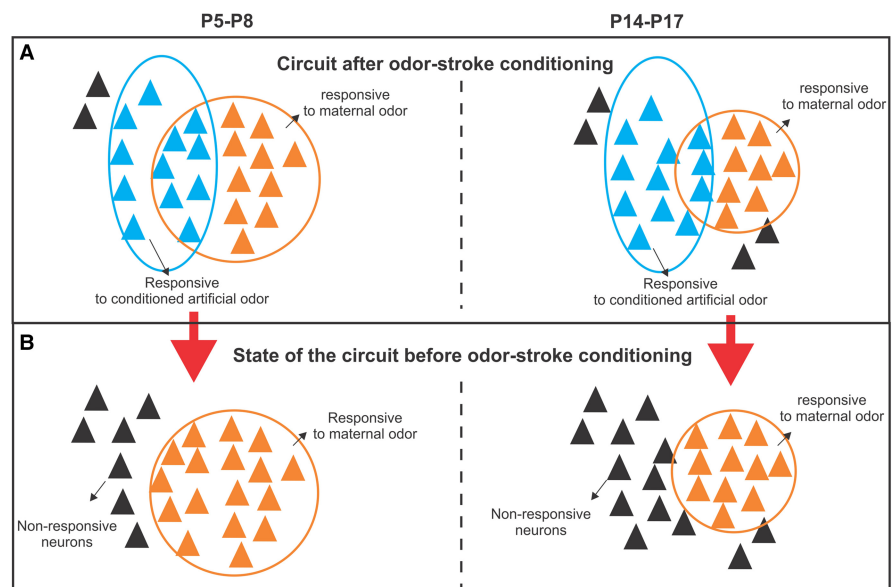

Figure 8. Graphical representations of the hypothesis. Some neurons that are responsive for an artificial odor may be coincident with neurons that are responsive to the maternal odor. This could occur to a lesser extent at P14–P17 than at P5–P8 (*A*). One possibility is that at P14–P17, the number of maternal odor responsive neurons could be reduced before the artificial odor-stroke conditioning in relation to P5–P8 (*B*).

700B amplifier (Molecular Devices). For current-clamp recording (Fig. 1A), the intracellular solution contained (in mM): potassium gluconate (120), KCl (10), MgCl$_2$ (1), CaCl$_2$ (0.025), EGTA (0.2), Na$_2$-ATP (2), Na$_2$-GTP (0.2), HEPES (10), titrated to pH 7.2 with KOH, and 290 mOsmol L^{-1}. Whole-cell recording pipettes had a tip resistance of 3–4 MΩ. Data were digitalized at 10 kHz with Digidata 1440-A System (Molecular Devices), filtered at 1 kHz (−3 dB, eight-pole Bessel) and analyzed offline with pClamp 10.6 software (Molecular Devices). The membrane potential was held at −65 mV for all neurons. Cells were excluded if they did not meet the following criteria: a stable resting membrane potential more negative than −55 mV, action potential crossing 0 mV. For measuring intrinsic properties of cells, a series of depolarizing and hyperpolarizing currents, 500 msec long, square-pulse current steps were injected (−180 pA to +300 pA) with intervals of 500 msec, steps of 20 pA.

Data analysis

The membrane resting potential (V$_{rest}$) was measured within a few minutes after breaking the membrane and defined as the steady-stable membrane potential (in the I = 0 mode). Input resistance (R$_{in}$) from the steady-stable voltage response to 1 sec of subthreshold current injection of −100 pA was calculated as the ratio of the peak voltage deflection to the current injected. The time constant (τ$_m$) was defined as the time necessary for the cell to reach 63.2% of its maximal deflection in response to hyperpolarizing current injection (−100 pA). The membrane capacitance (C$_m$) was calculated using the formula C$_m$ = τ$_m$/R$_{in}$. To measure action potentials (AP) a 1-sec long series of depolarizing steps were applied (range 20–300 pA, at 20 pA increments). Only APs with amplitudes above 10 mV were included in the analysis. Rheobase was defined as the minimal depolarizing current injected to generate at least one AP. The first spike evoked by a current step was used for the measurement of AP properties. The average AP amplitude was defined as the mean of the voltage increase from the AP threshold to the AP peak of the first spike amplitude for all depolarizing current injections. Average of the AP duration was defined as the full width at the half-maximal amplitude for the first spike of all depolarizing current injections. Spike frequency was calculated by quantifying the number of spikes elicited by 1-sec duration of depolarizing current injection. Interspike interval (ISI) was defined as the time between the peak of the first and the second AP. To characterize the pyramidal cell response in a time-window equivalent to the inhalation phase of the respiration cycle, we also quantified the number of spikes and the ISI at the first 200 msec from recordings with a 1-sec duration of depolarizing current injection.

All chemical substances used were obtained from Sigma–Aldrich. For statistical analysis, all data sets were tested for normality using the Kolmogorov–Smirnov test (α = 0.05) in Graph Prism 6. The electrophysiological statistical analysis was performed using a two-tailed unpaired Student's t-test after the normality test. Significance was considered when $P < 0.05$. All values in text, figures, and table are given as mean ± SEM.

Computational model

We developed an integrated model of OB and aPC based on the models by de Almeida et al. (2013, 2016) to investigate (a) how the aPC P5–P8 and P14–P17 circuit learn olfactory preference for maternal odor inside the nest and (b) how aPC pyramidal cells in these age groups respond after exposure to the conditioned maternal odor.

The computational model and simulations were developed using NetLogo 6.0.4 Software (Wilensky, U. 1999. NetLogo. http://ccl.northwestern.edu/netlogo/. June 4, 2018). In the framework of NetLogo, each neuron was represented as an individual agent that processes information.

Model architecture and connectivity

The OB network incorporates only the mitral cells (Mt) described in the work of de Almeida et al. (2013, 2016). We considered 100

Mt cells, and these were modeled with their firing dependent on the respiratory rhythm (2 Hz).

The aPC network is comprised only by pyramidal cells (Pyr) (Stokes and Isaacson 2010; Bekkers and Suzuki 2013) and consists of 200 neurons. We added experimental data (results reported in this paper) to the model. Passive (membrane resting potential, input resistance, membrane time constant, membrane capacitance) and active (AP threshold, AP amplitude, AP duration, AP firing frequency) intrinsic properties of aPC pyramidal cells were included from patch-clamp experimental data.

For the connectivity between OB and aPC, we considered that each Pyr cell is randomly connected with ~15 to 45 Mt cells (Franks and Isaacson 2006). For the associative Pyr–Pyr connectivity, we considered that each Pyr cell is connected randomly with 10% of Pyr cells (Franks et al. 2011). All parameters are presented in Table 2.

Models for the neurons and connections

The Mt and Pyr cells are modeled as leaky integrate-and-fire neurons, in which the change in the membrane voltage is described by the equation (1):

$$\frac{dV(t)}{dt} = \frac{1}{C}(I_e(t) - g_L(V(t) - E_L)), \qquad (1)$$

where V (t) is the membrane potential, C is the capacitance, g$_L$ is the membrane leaky conductance, E$_L$ is the resting potential, and I_e is the time-dependent external current input. To maintain the adjusted form of the experimental data for ISI and conserve the distribution for aPC pyramidal cells for each age period, I_e was multiplied by an adaptation factor α.

The external input (I^{ij}_e) to neuron i from a given presynaptic neuron j at time t is a function of the synaptic strength (W$_{ij}$), the channel conductance g$_{ij}$ (t) at time t, and the difference between the equilibrium potential (Nernst) (E$_{N,ij}$) of the specific channel

Table 2. Modeling parameters for P5–P8 and P14–P17

Neurons	P5–P8	P14–P17
Mitral Cells (Mt) (n = 100)	τ = 20 msec	
	Θ$_{min}$ = −0.0014; Θ$_{max}$ = 0.009[a]	
	Θ$_{min}$ = −0.0014; Θ$_{max}$ = 0.002[b]	
	V$_{hyper}$ = −0.01; t^{refrac} = 2 msec	
Pyramidal cells (Pyr) (n = 200)	Θ$_{min}$ = −0.03922 ; Θ$_{max}$ = −0.03663	Θ$_{min}$ = −0.05435; Θ$_{max}$ = −0.04596
	V^{hyper} = Θ$_{min}$; t^{refrac} = 2 msec	V^{hyper} = Θ$_{min}$; t^{refrac} = 2 msec
	τ = 42.78[c]	τ = 30.33[c]
	C$_m$ = 98.21[c]	C$_m$ = 178.1[c]
	R$_{inp}$ = τ/C$_m$[c]	R$_{inp}$ = τ/C$_m$[c]
	AP$_{ampl}$ = 0.07690[c]	AP$_{ampl}$ = 0.07690[c]
	E$_{pahp}$ = −0.060	E$_{pahp}$ = −0.060
	τ$_{pahp}$ = 1	τ$_{pahp}$ = 20
	A$_{pahp}$ = 30	A$_{pahp}$ = 30
	Rm$_{adapt}$ = 0.12	Rm$_{adapt}$ = 0.45
	W$_{Mt\ to\ Pyr}$ = 35	W$_{Mt\ to\ Pyr}$ = 35
	g^{max}$_{Pyr\ to\ Pyr}$ = 10	g^{max}$_{Pyr\ to\ Pyr}$ = 10
	W$_{Pyr\ to\ Pyr}$ = 35	W$_{Pyr\ to\ Pyr}$ = 35
	g^{max}$_{Mt\ to\ Pyr}$ = 10	g^{max}$_{Mt\ to\ Pyr}$ = 10
	E$_{glu}$ = 0	E$_{glu}$ = 0
	τ^{pp} = 12 msec	τ^{pp} = 12 msec
	τ^{pnp} = τ^{npp} = 500 msec	τ^{pnp} = τ^{npp} = 500 msec
	W$_{LTP}$ = 62.2	W$_{LTP}$ = 62.2
	W$_{LTD}$ = 12.25	W$_{LTD}$ = 12.25

[a]Values without NE modulation.
[b]Values with NE modulation.
[c]Values from electrophysiological data.

type and the membrane potential $V_i(t)$ of the postsynaptic neuron at time t and is described by the equation (2):

$$I_e^{ij}(t) = W_{ij}g_{ij}(t)[E_{N,ij} - V_i(t)]. \qquad (2)$$

The firing probability of the model neuron at voltage V is described by the equation (3):

$$F_i(V) = \begin{cases} 0 & \text{if } V < \theta^{min} \\ \left(\dfrac{V - \theta^{min}}{\theta^{max} - \theta^{min}}\right)^{\beta} & \text{if } V \in [\theta^{min}, \theta^{max}], \\ 1 & \text{if } V > \theta^{max} \end{cases} \qquad (3)$$

where θ^{max} represents the saturation value of threshold, θ^{min} is the minimal value of threshold, and β is a constant defining the nonlinearity of $F_i(V)$. At each spike of the presynaptic neuron j the corresponding conductance in the postsynaptic neuron i is set to:

$$g_{ij}(t) = g_{ij}^{max}\left(\exp\left(\frac{t - t_j^{fire}}{\tau_{1,ij}}\right) - \exp\left(-\frac{t - t_j^{fire}}{\tau_{2,ij}}\right)\right), \qquad (4)$$

where t_j^{fire} is the last spike time of neuron j, g_{ij}^{max} represents the maximum conductance of the corresponding channel, while $\tau_{1,ij}$ and $\tau_{2,ij}$ are its rise and fall. Following an action potential, the voltage of each neuron is reset to the hyperpolarization potential V^{hyper}, where it remains clamped for the refractory period $t^{refract}$.

We also implemented adaptation for the Pyr cells defined as a change in the voltage $V_i^{ahc}(t)$ due to a hyperpolarizing current that increases the firing threshold for the recently activated Pyr neurons i and it is described by the equation (5):

$$\tau^{ahc}\frac{dV_i^{ahc}}{dt} + V_i^{ahc} = A^{ahc}X_i, \qquad (5)$$

where X_i is equal to 1 in the time-step after neuron i spikes and 0 otherwise. Therefore, V^{ahc} increases with the constant A^{ahc} and decays with the characteristic time τ^{ahc} (de Almeida et al. 2013, 2016).

In the model, the excitatory output from Mt cells is modulated by the sinusoidal wave of 2 Hz, which mimics the respiratory rhythm (Uchida and Mainen 2003; Kepecs et al. 2007; Verhagen et al. 2007; Wesson et al. 2008; Poo and Isaacson 2009). The duration of each respiratory cycle was based on in vivo experimental works in rodents (Poo and Isaacson 2009; Haddad et al. 2013; Stern et al. 2018) and the beginning of the odor stimulation was programmed to coincide with the beginning of the exhalation phase.

Experimental works have shown that odor-stroke pairing enhances the OB activity in <P10 infant rodents (Sullivan and Wilson 1991a,b, 1995) and that at the same time the level of NE increases (Rangel and Leon 1995). NE release is necessary for the acquisition of olfactory preference in infant rodents, the behavioral orientation-approximation response to the conditioned odor (Sullivan et al. 1991, 2000; Sullivan and Wilson 1991a). The blockage of β-adrenoceptors in the OB (Sullivan et al. 1992) or a lesion of LC, blocking NE release, prevents this learning (Sullivan et al. 1994) and rat pups do not show olfactory preference for the conditioned odor. The presence of NE during odor presentation maintains Mt cells responsiveness to that odor, preventing the habituation they normally exhibit to repeated odor presentations (Wilson and Sullivan 1992). Therefore, we model the circuit so that during the conditioning experiments NE modulates only OB mitral cells.

Model for synaptic plasticity

For synaptic modifications of Mt to Pyr and Pyr to Pyr connections, activity-dependent synaptic plasticity was implemented (Hebbian learning) similar to that used by Jensen et al. (1996). The synaptic strength W_{ij} is increased if both pre- and postsynaptic neurons fire together; otherwise, it is reduced. This change is described by equation (6):

$$\frac{dW_{ij}}{dt} = (W_{LTP} - W_{ij})\frac{i^{post}(t - t_i^{fire})b^{glu}(t - t_j^{fire} - t^{delay})}{\tau^{pp}} \\ + (W_{LTD} - W_{ij})\left(\frac{i^{post}(t - t_i^{fire})}{\tau^{npp}} + \frac{b^{glu}(t - t_j^{fire} - t^{delay})}{\tau^{pnp}}\right) \qquad (6)$$

where t^{delay} is the time required for the action potential to travel from the soma to the recurrent collateral connections, i^{post} is the postsynaptic depolarization attributed to the retropropagated action potential of postsynaptic neurons described by equation (7):

$$i^{post}(t) = \frac{t}{\tau^{post}}\exp\left(1 - \frac{t}{\tau^{post}}\right), \qquad (7)$$

where the time course of the depolarization at the postsynaptic neuron (τ^{post}) is 2 msec. b^{glu} is the time course of the kinetics of the binding of glutamate on NMDA receptors (de Almeida et al 2013, 2016) described by equation (8).

$$b^{glu}(t) = \exp\left(\frac{-t}{\tau^{NMDAf}}\right)\left(1 - \exp\left(\frac{-t}{\tau^{NMDAr}}\right)\right), \qquad (8)$$

where τ^{NMDAf} (7 msec) and τ^{NMDAr} (1 msec) characterize the NMDA receptor kinetics.

During the first postnatal weeks, NMDA receptors are predominant at the LOT-aPC synapses (Mt–Pyr) (Franks and Isaacson 2005), which express a robust NMDA-dependent LTP plasticity but whose strength declines by the first postnatal month. The associative synapses (Pyr to Pyr), on the other hand, are always plastic (Poo and Isaacson 2007). In the simulation, the initial weight value (W) was set to 35, and the maximum weight value (W_{LTP} and the minimum value (W_{LTD} was set to 62.2 and 12.25, respectively). If i^{post} and b^{glu} peak together, then the synaptic weight between the neurons i and j is driven to W_{LTP} with the characteristic time τ^{pp} (12 msec) otherwise, in the case of unsynchronized firing, it is slowly reduced to W_{LTD} with the time constants $\tau^{pnp} = \tau^{npp} = 500$ msec.

Conditioning

After the model of the OB-aPC circuit was implemented for P5–P8 and P14–P17 age periods, we simulated a classical conditioning protocol. It assumes that by the time the younger pups (<P10) are submitted to the pairing of a novel odor with stroke (a tactile stimulus that mimics maternal licking), they already have learned in the nest the mother's odor. The conditioned maternal odor elicits in the pup an orientation-approximation behavior. At the circuit level, the coincidental activation of the same group of aPC neurons responsive for this behavior toward the mother odor supports the acquisition of a preference for a conditioned novel odor in young pups (<P10) in experimental conditions outside the nest. Conversely, preference learning for a novel artificial odor fails for older pups (>P10) because the stroke-odor pairing recruits less aPC neurons that are sensitive to the maternal odor.

We hypothesized that aPC Pyr cells are less responsive to odor-stroke conditioning after P10 because they become less responsive to the maternal odor with the changes in their intrinsic electric properties. Pyr cells in other sensory cortices become more adult-like around the first postnatal month (Lorenzon and Foehring 1993; Kasper et al. 1994; Maravall et al. 2004; Oswald and Reyes 2008; Valiullina et al. 2016). Moreover, in recent electrophysiological studies, aPC Pyr cells of mice have been found to undergo developmental changes in their intrinsic passive and action potential properties from P8–P11 to P14–P21 (Ghosh et al. 2015). In this paper, we show that from P5–P8 to P14–P17, the resting membrane potential, the input resistance, and the membrane time constant have an important reduction. Moreover, the Pyr cells

APs reduce in threshold and become faster with age but with little change in amplitude.

In our simulation of the classical conditioning protocol, the OB-aPC model initially receives the mother's odor as a neutral stimulus. Before CS–USC pairing, the response of aPC pyramidal cells to the maternal odor was measured in a 3 sec window with 2 sec of interval. In the delayed pairing procedure, the CS onset preceded the UCS onset by 2 sec, CS–USC overlapping for 1 sec, after which the CS was terminated. This pairing was presented seven times with 1-sec intervals. During this procedure, we measured the activity of the pyramidal cells (number of spikes, number of activated cells, and change in the synaptic weight). Two seconds after the last pairing, the CS was presented alone during a 3-sec window.

After the pup has learned the mother`s odor by conditioning (representing pups <P10), exposure to this conditioned odor is expected to elicit orientation-approximation behavior, and at the neural level, it is expected that specific aPC pyramidal cells are highly active. To illustrate this, we exposed the P5–P8 OB-aPC artificial circuit to the CS stimuli for a 10-sec window and measured the activity of the Pyr cells during this period. After a 2 sec interval, we exposed the P5–P8 OB-aPC circuit again during a 3-sec window to the CS and measure the aPC pyramidal cells activity.

In the >P10 pups, exposure to the maternal odor also elicits orientation-approximation behavior (Sullivan et al. 1986; Sullivan and Wilson 1993), but the novel odor repetitively paired with stroke does not induce any of this behavior (Moriceau and Sullivan 2005). We hypothesized that the specific aPC pyramidal cells that were highly active in <P10 pups should have been reduced in >P10 pups. To test this hypothesis, we switched the electrophysiological characteristic of the pyramidal cells from P5–P8 to P14–P17 and exposed the circuit to the CS during a 10 sec time-window and measured the activity of the aPC pyramidal cells. After a 2-sec interval, another 3 sec of CS exposure was measured 2 sec after the first exposure.

Acknowledgments

References

Al Aïn S, Perry RE, Nuñez B, Kayser K, Brehman E, Lacomb M, Wilson DA, Sullivan RM. 2016. Neurobehavioral assessment of maternal odor in developing rat pups: implications for social buffering. *Soc Neurosci* **12**: 32–49. doi:10.1080/17470919.2016.1159605

Bekkers JM, Suzuki N. 2013. Neurons and circuits for odor processing in the piriform cortex. *Trends Neurosci* **36**: 429–438. doi:10.1016/j.tins.2013 .04.005

Choy JMC, Suzuki N, Shima Y, Budisantoso T, Nelson SB, Bekkers JM. 2017. Optogenetic mapping of intracortical circuits originating from semilunar cells in the piriform cortex. *Cerebral Cortex* **27**: 589–601. doi:10.1093/cercor/bhv258

Cornwell-Jones C, Sobrian SK. 1977. Development of odor-guided behavior in Wistar and Spraque-Dawley rat pups. *Physiol Behav* **19**: 685–688. doi:10.1016/0031-9384(77)90044-0

de Almeida L, Idiart M, Linster C. 2013. A model of cholinergic modulation in olfactory bulb and piriform cortex. *J Neurophysiol* **109**: 1360–1377. doi:10.1152/jn.00577.2012

de Almeida L, Idiart M, Dean O, Devore S, Smith DM, Linster C. 2016. Internal cholinergic regulation of learning and recall in a model of

olfactory processing. *Front Cell Neurosci* **10**: 1–14. doi:10.3389/fncel .2016.00256

Donahoe JW, Burgos JE, Palmer DC. 2006. A selectionist approach to reinforcement. *J Exp Anal Behav* **60**: 17–40. doi:10.1901/jeab.1993.60-17

Duveau A, Godinot F. 1988. Influence of the odorization of the rearing environment on the development of odor-guided behavior in rat pups. *Physiol Behav* **42**: 265–270. doi:10.1016/0031-9384(88)90080-7

Franks KM, Isaacson JS. 2005. Synapse-specific downregulation of NMDA receptors by early experience: a critical period for plasticity of sensory input to olfactory cortex. *Neuron* **47**: 101–114. doi:10.1016/j.neuron .2005.05.024

Franks KM, Isaacson JS. 2006. Strong single-fiber sensory inputs to olfactory cortex: implications for olfactory coding. *Neuron* **49**: 357–363. doi:10 .1016/j.neuron.2005.12.026

Franks KM, Russo MJ, Sosulski DL, Mulligan AA, Siegelbaum SA, Axel R. 2011. Recurrent circuitry dynamically shapes the activation of piriform cortex. *Neuron* **72**: 49–56. doi:10.1016/j.neuron.2011.08.020

Ghosh A, Purchase NC, Chen X, Yuan Q. 2015. Norepinephrine modulates pyramidal cell synaptic properties in the anterior piriform cortex of mice: age-dependent effects of β-adrenoceptors. *Front Cell Neurosci* **9**: 450. doi:10.3389/fncel.2015.00450

Ghosh A, Mukherjee B, Chen X, Yuan Q. 2017. β-adrenoceptor activation enhances L-type calcium channel currents in anterior piriform cortex pyramidal cells of neonatal mice: implication for odor learning. *Learn Mem* **24**: 132–135. doi:10.1101/lm.044818.116

Gregory EH, Pfaff DW. 1971. Development of olfactory-guided behavior in infant rats. *Physiol Behav* **6**: 573–576. doi:10.1016/0031-9384(71) 90208-3

Haddad R, Lanjuin A, Madisen L, Zeng H, Murthy VN, Uchida N. 2013. Olfactory cortical neurons read out a relative time code in the olfactory bulb. *Nat Neurosci* **16**: 949–957. doi:10.1038/nn.3407

Jensen O, Idiart MAP, Lisman JE. 1996. Physiologically realistic formation of autoassociative memory in networks with θ/γ oscillations: role of fast NMDA channels. *Learn Mem* **3**: 243–256. doi:10.1101/lm.3.2-3.243

Kasper EM, Larkman AU, Lübke J, Blakemore C. 1994. Pyramidal neurons in layer 5 of the rat visual cortex. II. Development of electrophysiological properties. *J Comp Neurol* **339**: 475–494. doi:10.1002/cne.903390403

Kepecs A, Uchida N, Mainen ZF. 2007. Rapid and precise control of sniffing during olfactory discrimination in rats. *J Neurophysiol* **98**: 205–213. doi:10.1152/jn.00071.2007

Kimura F, Nakamura S. 1985. Locus coeruleus neurons in the neonatal rat: electrical activity and responses to sensory stimulation. *Dev Brain Res* **23**: 301–305. https://doi.org/10.1016/0165-3806(85)90055-0

Lorenzon NM, Foehring RC. 1993. The ontogeny of repetitive firing and its modulation by norepinephrine in rat neocortical neurons. *Dev Brain Res* **73**: 213–223. https://doi.org/10.1016/0165-3806(93)90141-V

Maravall M, Stern EA, Svoboda K. 2004. Development of intrinsic properties and excitability of layer 2/3 pyramidal neurons during a critical period for sensory maps in rat barrel cortex. *J Neurophysiol* **92**: 144–156. https://doi.org/10.1152/jn.00598.2003

McCormick DA, Prince DA. 1987. Post-natal development of electrophysiological properties of rat cerebral cortical pyramidal neurones. *J Physiol* **393**: 743–762. https://doi.org/10.1113/jphysiol .1987.sp016851

Moriceau S, Sullivan RM. 2004. Unique neural circuitry for neonatal olfactory learning. *J Neurosci* **24**: 1182–1189. doi:10.1523/JNEUROSCI .4578-03.2004

Moriceau S, Sullivan RM. 2005. Neurobiology of infant attachment. *Dev Psychobiol* **47**: 230–242. doi:10.1002/dev.20093

Morrison GL, Fontaine CJ, Harley CW, Yuan Q. 2013. A role for the anterior piriform cortex in early odor preference learning: evidence for multiple olfactory learning structures in the rat pup. *J Neurophysiol* **110**: 141–152. https://doi.org/10.1152/jn.00072.2013

Oswald A-MM, Reyes AD. 2008. Maturation of intrinsic and synaptic properties of layer 2/3 pyramidal neurons in mouse auditory cortex. *J Neurophysiol* **99**: 2998–3008. doi:10.1152/jn.01160.2007

Pardo GVE, Lucion AB, Calcagnotto ME. 2018. Postnatal development of inhibitory synaptic transmission in the anterior piriform cortex. *Int J Dev Neurosci* **71**: 1–9. doi:10.1016/j.ijdevneu.2018.07.008

Perry RE, Al Aïn S, Raineki XC, Sullivan RM, Wilson DA. 2016. Development of odor hedonics : experience-dependent ontogeny of circuits supporting maternal and predator odor responses in rats. *J Neurosci* **36**: 6634–6650. doi:10.1523/JNEUROSCI.0632-16.2016

Polan HJ, Hofer MA. 1998. Olfactory preference for mother over home nest shavings by newborn rats. *Dev Psychobiol* **33**: 5–20. doi:10.1002/(SICI) 1098-2302(199807)33:1<5::AID-DEV2>3.0.CO;2-P

Polan HJ, Milano D, Eljuga L, Hofer MA. 2002. Development of rats' maternally directed orienting behaviors from birth to day 2. *Dev Psychobiol* **40**: 81–103. doi:10.1002/dev.10015

Poo C, Isaacson JS. 2007. An early critical period for long-term plasticity and structural modification of sensory synapses in olfactory cortex. *J Neurosci* **27**: 7553–7558. doi:10.1523/JNEUROSCI.1786-07.2007

Poo C, Isaacson JS. 2009. Odor representations in olfactory cortex: "sparse" coding, global inhibition, and oscillations. *Neuron* **62:** 850–861. doi:10.1016/j.neuron.2009.05.022

Rangel S, Leon M. 1995. Early odor preference training increases olfactory bulb norepinephrine. *Dev Brain Res* **85:** 187–191. doi:10.1016/0165-3806(94)00211-H

Roth TL, Raineki C, Salstein L, Perry R, Sullivan-Wilson TA, Sloan A, Lalji B, Hammock E, Wilson DA, Levitt P, et al. 2013. Neurobiology of secure infant attachment and attachment despite adversity: a mouse model. *Genes Brain Behav* **12:** 673–680. doi:10.1111/gbb.12067

Stern M, Bolding KA, Abbott L, Franks KM. 2018. A transformation from temporal to ensemble coding in a model of piriform cortex. *Elife* **7:** e34831. doi:10.7554/elife.34831

Stokes CCA, Isaacson JS. 2010. From dendrite to soma: dynamic routing of inhibition by complementary interneuron microcircuits in olfactory cortex. *Neuron* **67:** 452–465. doi:10.1016/j.neuron.2010.06.029

Sullivan RM. 2001. Unique characteristics of neonatal classical conditioning: the role of the amygdala and locus coeruleus. *Integr Physiol Behav Sci* **36:** 293–307. doi:10.1007/bf02688797

Sullivan RM, Wilson DA. 1991a. Neural correlates of conditioned odor avoidance in infant rats. *Behav Neurosci* **105:** 307–312. doi:10.1037/0735-7044.105.2.307

Sullivan RM, Wilson DA. 1991b. The role of norepinephrine in the expression of learned olfactory neurobehavioral responses in infant rats. *Psychobiology* **19:** 308–312. doi:10.3758/bf03332084

Sullivan RM, Wilson DA. 1993. Role of the amygdala complex in early olfactory associative learning. *Behav Neurosci* **107:** 254–263. doi:10.1037/0735-7044.107.2.254

Sullivan RM, Wilson DA. 1995. Dissociation of behavioral and neural correlates of early associative learning. *Dev Psychobiol* **28:** 213–219. doi:10.1002/dev.420280403

Sullivan RM, Hofer MA, Brake SC. 1986. Olfactory-guided orientation in neonatal rats is enhanced by a conditioned change in behavioral state. *Dev Psychobiol* **19:** 615–623. doi:10.1002/dev.420190612

Sullivan RM, McGaugh JL, Leon M. 1991. Norepinephrine-induced plasticity and one-trial olfactory learning in neonatal rats. *Dev Brain Res* **60:** 219–228. doi:10.1016/0165-3806(91)90050-S

Sullivan RM, Zyzak DR, Skierkowski P, Wilson DA. 1992. The role of olfactory bulb norepinephrine in early olfactory learning. *Dev Brain Res* **70:** 279–282. doi:10.1016/0165-3806(92)90207-D

Sullivan RM, Wilson DA, Lemon C, Gerhardt GA. 1994. Bilateral 6-OHDA lesions of the locus coeruleus impair associative olfactory learning in newborn rats. *Brain Res* **643:** 306–309. doi:10.1016/0006-8993(94)90038-8

Sullivan RM, Stackenwalt G, Nasr F, Lemon C, Wilson DA. 2000. Association of an odor with activation of olfactory bulb noradrenergic β-receptors or locus coeruleus stimulation is sufficient to produce learned approach responses to that odor in neonatal rats. *Behav Neurosci* **114:** 957–962. doi:10.1037/0735-7044.114.5.957

Szerzenie V, Hsiao S. 1977. Development of locomotion toward home nesting material in neonatal rats. *Dev Psychobiol* **10:** 315–321. doi:10.1002/dev.420100405

Terry LM, Johanson IB. 1996. Effects of altered olfactory experiences on the development of infant rats' responses to odors. *Dev Psychobiol* **29:** 353–377. doi:10.1002/(SICI)1098-2302(199605)29:4<353::AID-DEV4>3.0.CO;2-P

Uchida N, Mainen ZF. 2003. Speed and accuracy of olfactory discrimination in the rat. *Nat Neurosci* **6:** 1224–1229. doi:10.1038/nn1142

Valiullina F, Akhmetshina D, Nasretdinov A, Mukhtarov M, Valeeva G, Khazipov R, Rozov A. 2016. Developmental changes in electrophysiological properties and a transition from electrical to chemical coupling between excitatory layer 4 neurons in the rat barrel cortex. *Front Neural Circuits* **10:** 1. doi:10.3389/fncir.2016.00001

Verhagen JV, Wesson DW, Netoff TI, White JA, Wachowiak M. 2007. Sniffing controls an adaptive filter of sensory input to the olfactory bulb. *Nat Neurosci* **10:** 631–639. doi:10.1038/nn1892

Wesson DW, Donahou TN, Johnson MO, Wachowiak M. 2008. Sniffing behavior of mice during performance in odor-guided tasks. *Chem Senses* **33:** 581–596. doi:10.1093/chemse/bjn029

Wilson DA, Sullivan RM. 1992. Blockade of mitral/tufted cell habituation to odors by association with reward: a preliminary note. *Brain Res* **594:** 143–145. doi:10.1016/0006-8993(92)91039-H